

Modal affinities of endplate acetylcholine receptors caused by loop C mutations

Ridhima Vij,¹ Prasad Purohit,² and Anthony Auerbach²

¹Neuroscience Program and ²Department of Physiology, State University of New York at Buffalo, Buffalo, NY 14214

The time course of the endplate current is determined by the rate and equilibrium constants for acetylcholine receptor (AChR) activation. We measured these constants in single-channel currents from AChRs with mutations at the neurotransmitter-binding sites, in loop C. The main findings are: (a) Almost all perturbations of loop C generate heterogeneity in the channel open probability (“modes”). (b) Modes are generated by different affinities for ACh that can be either higher or lower than in the wild-type receptors. (c) The modes are stable, in so far as each receptor maintains its affinity for at least several minutes. (d) Different agonists show different degrees of modal activity. With the loop C mutation α P197A, there are four modes with ACh but only two with partial agonists. (e) The affinity variations arise exclusively from the $\alpha\delta$ -binding site. (f) Substituting four γ -subunit residues into the δ subunit (three in loop E and one in the $\beta 5$ – $\beta 5'$ linker) reduces modal activity. (g) At each neurotransmitter-binding site, affinity is determined by a core of five aromatic residues. Modes are eliminated by an alanine mutation at δ W57 but not at the other aromatics. (h) Modes are eliminated by a phenylalanine substitution at all core aromatics except α Y93. The results suggest that, at the $\alpha\delta$ agonist site, loop C and the complementary subunit surface can each adopt alternative conformations and interact with each other to influence the position of δ W57 with respect to the aromatic core and, hence, affinity.

INTRODUCTION

The endplate acetylcholine receptor (AChR) is a heteropentamer of subunit composition $\alpha_2\beta\delta\epsilon$ (adult) or $\alpha_2\beta\delta\gamma$ (fetal). Each receptor has two agonist-binding sites located in the extracellular domain at $\alpha\delta$ - and either $\alpha\epsilon$ - or $\alpha\gamma$ -subunit interfaces, and each site has a core of five aromatic residues (Fig. 1). In mouse AChRs, at the two adult sites ($\alpha\epsilon$ and $\alpha\delta$), α Y190, α Y198, and α W149 are the main sources of ACh affinity and together generate a resting equilibrium K_d of ~ 150 μ M (Jadey et al., 2011; Purohit et al., 2012; Nayak et al., 2014). At the fetal $\alpha\gamma$ site, α Y93 and especially γ W55 also contribute to increase the resting affinity for ACh to ~ 5 μ M.

The principal (α -subunit) side of each agonist site is formed by loops A, B, and C. Loop C covers the binding pocket and contains α Y190 and α Y198 residues that make approximately the same contribution to affinity at all three kinds of agonist site ($\alpha\epsilon$, $\alpha\gamma$, and $\alpha\delta$). The removal of loop C does not affect constitutive gating but eliminates the agonist response (Purohit and Auerbach, 2013). The complementary (non- α -subunit) side of each agonist site is a super-secondary structure that is mostly β sheet. The higher resting affinity of the fetal $\alpha\gamma$ site is set by residues in loop E and the $\beta 5$ – $\beta 5'$ linker, which influence the contribution of γ W55 (W57 in the δ subunit; unpublished data).

The consistency of a synaptic response depends, in part, on the consistency of the underlying binding and gating rate and equilibrium constants that shape the current. Hence, different open probability (P_o) modes of activation will generate different synaptic responses. Single-channel modes have been reported for several different WT synaptic receptors, including for ACh (Auerbach and Lingle, 1986; Naranjo and Brehm, 1993), GABA (Lema and Auerbach, 2006), glycine (Hurdiss et al., 2015), AMPA (Poon et al., 2010; Prieto and Wollmuth, 2010), and NMDA (Popescu and Auerbach, 2003; Magleby, 2004; Zhang et al., 2008). Mode shifts have also been observed in other WT ion channels (Blatz and Magleby, 1986; Nilius, 1987; McManus and Magleby, 1988; Smith and Ashford, 1998; Ionescu et al., 2007; Chakrapani et al., 2011). It is of general interest to understand the molecular basis of modal activity, even if this may arise by different mechanisms in different ion channels.

We have explored the effects of mouse endplate AChR loop C mutations with regard to the consistency of binding and gating constants, estimated from single-channel currents. Almost all α -loop C perturbations unsettle resting affinity and generate distinct, stable P_o modes. The affinity variations arise exclusively at the $\alpha\delta$ agonist site, with patterns that are different for different agonists. We explore a possible mechanism in which α -loop

Correspondence to Anthony Auerbach: auerbach@buffalo.edu

Abbreviations used in this paper: AChR, acetylcholine receptor; P_o , open probability; TMA, tetramethylammonium.

© 2015 Vij et al. This article is distributed under the terms of an Attribution–Noncommercial–Share Alike–No Mirror Sites license for the first six months after the publication date (see <http://www.rupress.org/terms>). After six months it is available under a Creative Commons License (Attribution–Noncommercial–Share Alike 3.0 Unported license, as described at <http://creativecommons.org/licenses/by-nc-sa/3.0/>).

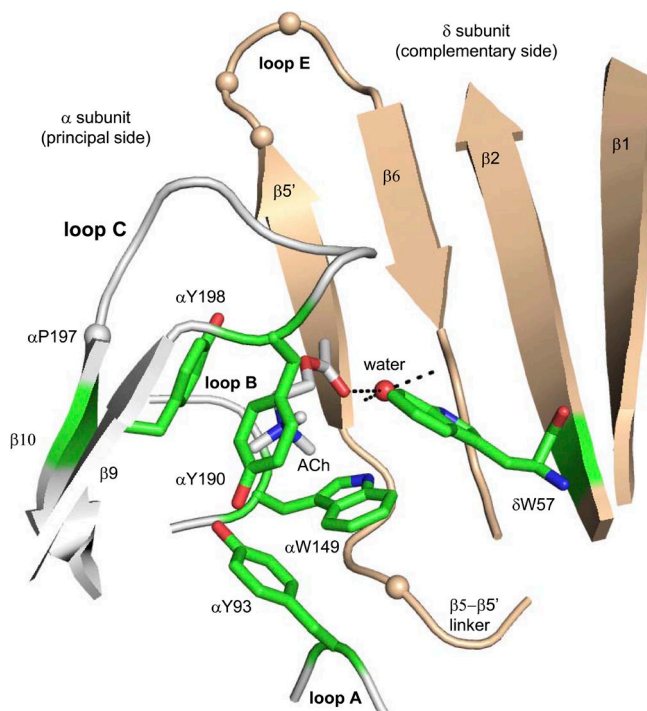


Figure 1. The ligand-binding site of an acetylcholine binding protein. The agonist-binding sites are at subunit interfaces; the principal side (α subunit in AChRs) is white, and the complementary side (δ , ϵ , or γ subunit) is tan. The structure is *Lymnaea stagnalis* (Protein Data Bank accession no. 3WIP; Olsen et al., 2014), and residue numbers are mouse endplate AChRs. Green, aromatic core; tan spheres, α C atoms of γ -subunit substitutions (see Fig. 6); red sphere, structural water; dashed lines, H bonds.

C and the δ -subunit β sheet each take on alternative conformations to set the structure of the aromatic core and affinity.

MATERIALS AND METHODS

Cell culture and mutagenesis

HEK293 cells were maintained in DMEM supplemented with 10% (vol/vol) fetal bovine serum plus 1% (vol/vol) penicillin-streptomycin, pH 7.4, and were incubated at 37°C (5% CO₂). The Quick-Change site-directed mutagenesis kit (Agilent Technologies) was used to incorporate mutations into the mouse AChR cDNAs, which were verified by nucleotide sequencing. Transient transfection of cDNAs into HEK293 cells was either by a calcium phosphate precipitation method or by using TransIT-293 transfection reagent (Mirus). After transfection, cells were incubated for ~16–24 h at 37°C before electrophysiological recordings commenced.

Electrophysiology

Single-channel currents were recorded at 23°C in the cell-attached patch configuration. The bath solution was Dulbecco's PBS containing 137 mM NaCl, 0.9 mM CaCl₂, 2.7 mM KCl, 1.5 mM KH₂PO₄, 0.5 mM MgCl₂, and 8.1 mM Na₂HPO₄, pH 7.4. The pipette solution was PBS. In some experiments, an agonist (acetylcholine, carbamylcholine, tetramethylammonium [TMA], or choline) was added only to the pipette solution. For experiments without ligands, we used a pipette holder and electrode that were never exposed

to any agonists. When low [agonist] were used, the pipette potential was 70 mV, which corresponds to a membrane potential of approximately -100 mV (inward currents). When high [agonist] were used, the pipette potential was -100 mV, which corresponds to a membrane potential of approximately 70 mV (outward currents) to reduce channel block by the agonist. When necessary, rate constants were corrected for the effect of voltage (Nayak et al., 2012). Single-channel currents were low-pass filtered at 20 kHz and digitized at a sampling frequency of 50 kHz. Collection and analyses of the currents were performed using QuB software (Nicolai and Sachs, 2013).

Cluster selection and K_d/P_O estimation

Single-channel currents associated with $C \leftrightarrow O$ gating occur as clusters separated by long desensitized periods (Sakmann et al., 1980). Sometimes, a t_{crit} value of 6.5 ms was used to define a cluster (for example, Fig. 2 A). However, there often was a wide distribution of intra-cluster shut-interval durations making it impossible to use a single t_{crit} value (Fig. 2 B). In these patches, clusters were selected by eye. In either case, a k-means clustering algorithm was applied to the selected clusters to determine the number of P_O populations and to segregate the clusters for mode-by-mode analysis.

For rate constant estimation, intra-cluster currents for each P_O population were idealized into noise-free intervals by using the segmental k-means algorithm, after low-pass filtering at 12 kHz. The forward (f) and backward (b) gating rate constants were estimated from the interval durations by fitting with a $C \leftrightarrow O$ model and a maximum-interval likelihood algorithm after imposing a dead time of 20–50 μ s. Occasionally, an additional shut state was added to account for a short-lived desensitized state (Elenes and Auerbach, 2002). The gating equilibrium constant was calculated from the ratio of the rate constants, $E_n = f_n/b_n$, where n is the number of bound agonists. P_O was calculated from the gating equilibrium constant, $P_O = (1 + E_n)^{-1}$. For unliganded gating, E_0 was calculated from the ratio of closed-/open-time constant, using the main component of each interval duration histogram.

AChR gating is described by a cyclic mechanism (Auerbach, 2012). In brief, WT receptors are active constitutively but with a small unliganded gating equilibrium constant (allosteric constant) that generates a very low P_O (Jackson, 1986; Purohit and Auerbach, 2009; Nayak et al., 2012). P_O is increased by agonists because these ligands bind with a higher affinity to the O versus C conformation. Accordingly, the gating equilibrium constant with one bound agonist (E_1) is the product of the gating equilibrium constant without any agonists (E_0) and the C/O equilibrium dissociation constant ratio. Cluster P_O with agonists is a function of both resting affinity (K_d) and the allosteric constant (E_0).

A shortcut was used to estimate K_d . This was possible because in mouse endplate AChRs, affinity and efficacy are correlated (Jadey and Auerbach, 2012; Purohit et al., 2014). With n equal-affinity neurotransmitter-binding sites, the resting affinity K_d can be calculated from the unliganded and fully liganded gating equilibrium constants by using:

$$K_d = (E_0/E_n)^{1/n}. \quad (1)$$

For example, in adult WT AChRs (-100 mV), $n = 2$, $E_0 = 7.4 \times 10^{-7}$, and $E_2^{ACh} = 25$, so from Eq. 1, we calculate $K_d^{ACh} = 172 \mu$ M, which is about the same as that measured by standard dose-response methods (Jadey et al., 2011).

Backgrounds

In many experiments, the goal was simply to count the number of cluster P_O populations. To facilitate this enumeration, a background mutation(s) was often added simply to increase E_0 and place the shut and open intervals into an optimal range for cluster formation

and P_O analysis (Jadey et al., 2011). In these cases, it was not necessary to know the quantitative effect of the background on E_0 . For example, for WT adult AChRs, E_0 is small (the shut intervals between openings are long) and clusters cannot be defined. To increase the unliganded channel-opening frequency, we added two background mutations, β L262G and δ L265G, both far away from the binding site at the M2 gate region. This pair of mutations increased the unliganded opening rate constant by $\sim 26,000$ -fold, to reveal clusters having P_O of ≈ 0.02 (Fig. 3 A, top).

The background mutations used to increase E_0 (by x-fold) and facilitate cluster counting are as follows: Fig. 4 B, ϵ S450W (9.95-fold); Fig. 5, ϵ S450A (17-fold); Fig. 6, either δ (P123R + W57A) to

knock-out the $\alpha\delta$ site (0.06-fold), or ϵ P121R to knock-out the $\alpha\epsilon$ site (0.09-fold; Gupta et al., 2013) plus β V266A (446-fold; Fig. 6, A and C), β V266A + ϵ S450W (4438-fold; Fig. 6 B, top), or γ L260Q (3,570-fold; Fig. 6 B, bottom); Fig. 7, α C192A and α C193A (ϵ S450A), α Y190A (α D97A + α Y127F + ϵ S450W; 98,600-fold), α Y198A, α C192 deletion, and α T196F (ϵ L269F; 176.8-fold); Fig. 8 A, the $\alpha\epsilon$ knockout mutations plus ϵ L269F; Fig. 8 B, for α W149A and α Y198A (ϵ L269F) and for α Y93A (ϵ S450A); Fig. 9 A, for α Y190F and α W149F (ϵ L269F); Fig. 9, the $\alpha\epsilon$ knockout plus for α Y190F (δ L265G + δ I43Q + ϵ L269F; 1.10^3 -fold), for α Y198F (δ I43Q + ϵ L269F; 81-fold), and for δ W57F (ϵ L269F). In all other experiments, the background was adult WT. Again, all of the

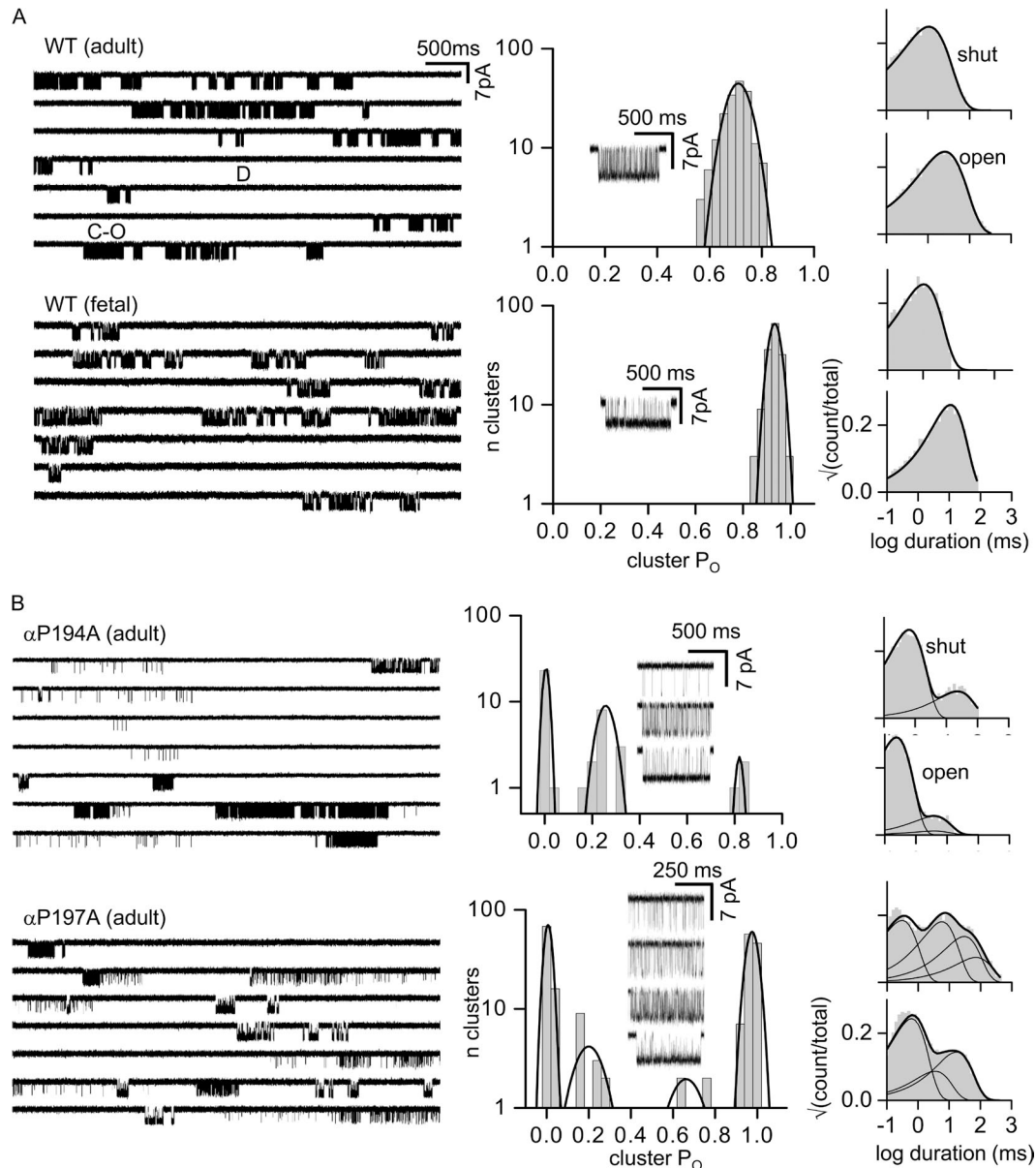


Figure 2. Loop C proline mutations generate P_O modes. WT AChR clusters are homogenous. (A; left) Single-channel currents (30 μ M ACh; -100 mV; open is down). Clusters of openings are binding-gating events (C-O) and long silent intervals between clusters are desensitization (D). (Right) Histograms of cluster P_O (fitted by a single Gaussian) and intra-cluster interval durations (fitted by a single exponential). (Inset) An example cluster. In both adult and fetal AChRs, there is only a single P_O population (0.70 ± 0.06 , 187, and 0.93 ± 0.03 , 156; mean \pm SD; n clusters). (B) Loop C mutations α P197A and α P194A in adult AChRs induce modes. P_O histograms for α P197A have four populations (0.01 ± 0.01 , 83; 0.20 ± 0.04 , 6; 0.67 ± 0.06 , 8; and 0.96 ± 0.01 , 110), and multiple exponentials are required to describe the interval duration distributions.

backgrounds only served to increase E_0 to enhance cluster formation (Jadey et al., 2011).

To estimate K_d for different modes (Table 1), it was necessary to know both E_1 and E_0 (Eq. 1). We added a background mutation(s) that increased E_0 over the adult WT value, each by a known factor. When multiple mutations were added, we assumed that the effects were independent, so that the product of the individual fold-changes estimated the combined effect. E_2 was estimated from the measured values of f_n and b_n , as described above.

RESULTS

Modes

Fig. 2 A shows ACh-activated single-channel currents from WT AChRs. Openings occur in clusters that contain many cycles of binding and gating, and that are separated by long, silent sojourns in desensitized states. In both adult and fetal AChRs, the distribution of intra-cluster P_O was approximately Gaussian and consistent, patch-to-patch. In some recordings, there were also isolated, brief openings interspersed between the clusters. Aside from these, the single-channel current

properties of adult and fetal WT AChRs are essentially homogeneous.

In mouse endplate AChRs, α -subunit loop C ($\beta 9$ – $\beta 10$ linker) has the sequence VFYSCCPTTPYL ($\alpha 188$ – $\alpha 199$). We first examined the effects of alanine substitutions at either of the two prolines (Fig. 2 B). Unlike in the WT, clusters from adult AChRs having the mutation $\alpha P194A$ or $\alpha P197A$ showed a multimodal distribution of P_O^{ACh} values. In $\alpha P197A$, there are four different cluster populations (modes) having P_O values between 0.01 and 0.96, in addition to isolated openings.

Heterogeneity in P_O can be caused by differences in gating (the allosteric constant, which is the unliganded gating equilibrium constant; see Materials and methods), the resting affinity (K_d), or both. We therefore examined $\alpha P194A$ and $\alpha P197A$ clusters without adding any agonists (Fig. 3). To do so, we added background mutations far from the agonist sites that increased the level of constitutive activity but had no effect on K_d . The loop C mutations $\alpha P194A$ or $\alpha P197A$ had no or little effect on the allosteric constant. Moreover, neither of these loop C proline mutations resulted in unliganded P_O heterogeneity.

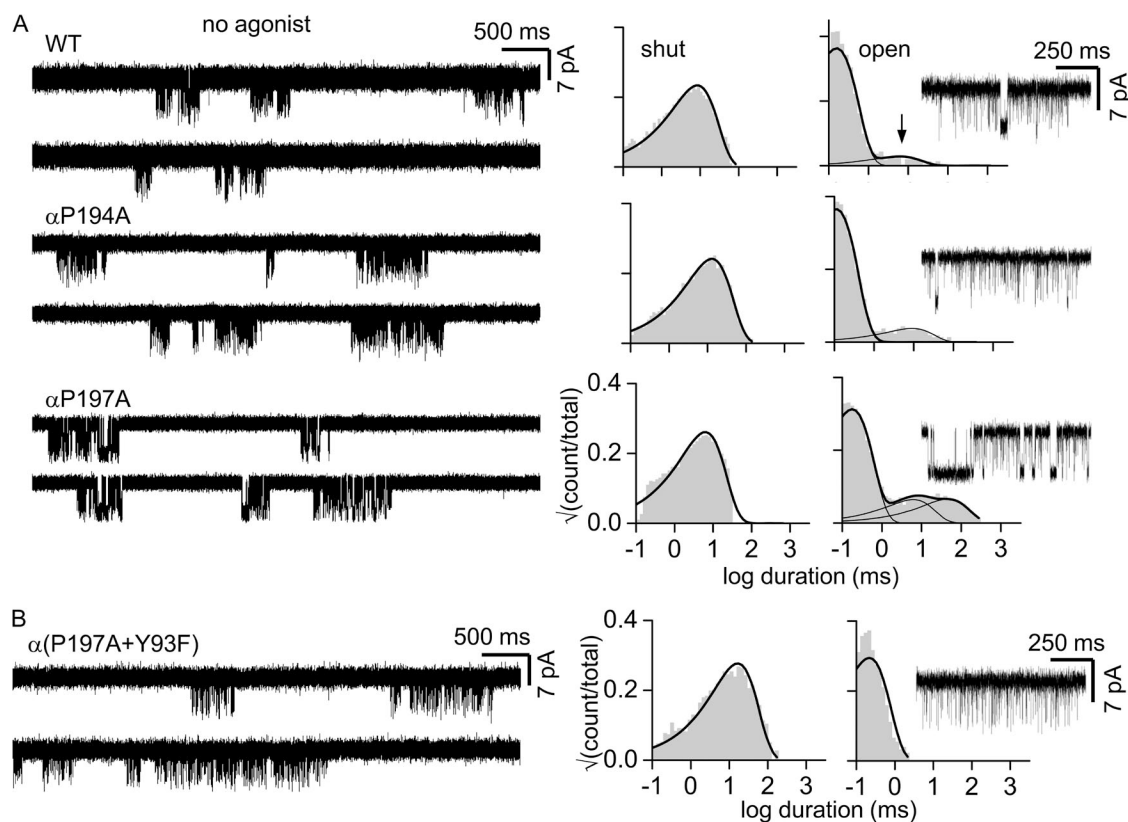


Figure 3. Gating of loop C proline mutants in the absence of agonists is homogeneous. (A; left) Single-channel clusters from unliganded AChRs (adult type, -100 mV; background mutation were added to increase constitutive activity; see Materials and methods). (Right) Intra-cluster interval duration histograms and an example cluster. WT, $\alpha P194A$, and $\alpha P197A$ show both brief and long (arrow) unliganded openings. The briefer, main component of each distribution represents C-O gating; the longer open component(s) is characteristic of unliganded activity but is distinct from C-O and of unknown origin (Purohit and Auerbach, 2009). (B) Adding the agonist site mutation $\alpha Y93F$ eliminates long unliganded openings but does not affect the gating open interval time constant (Purohit and Auerbach, 2010).

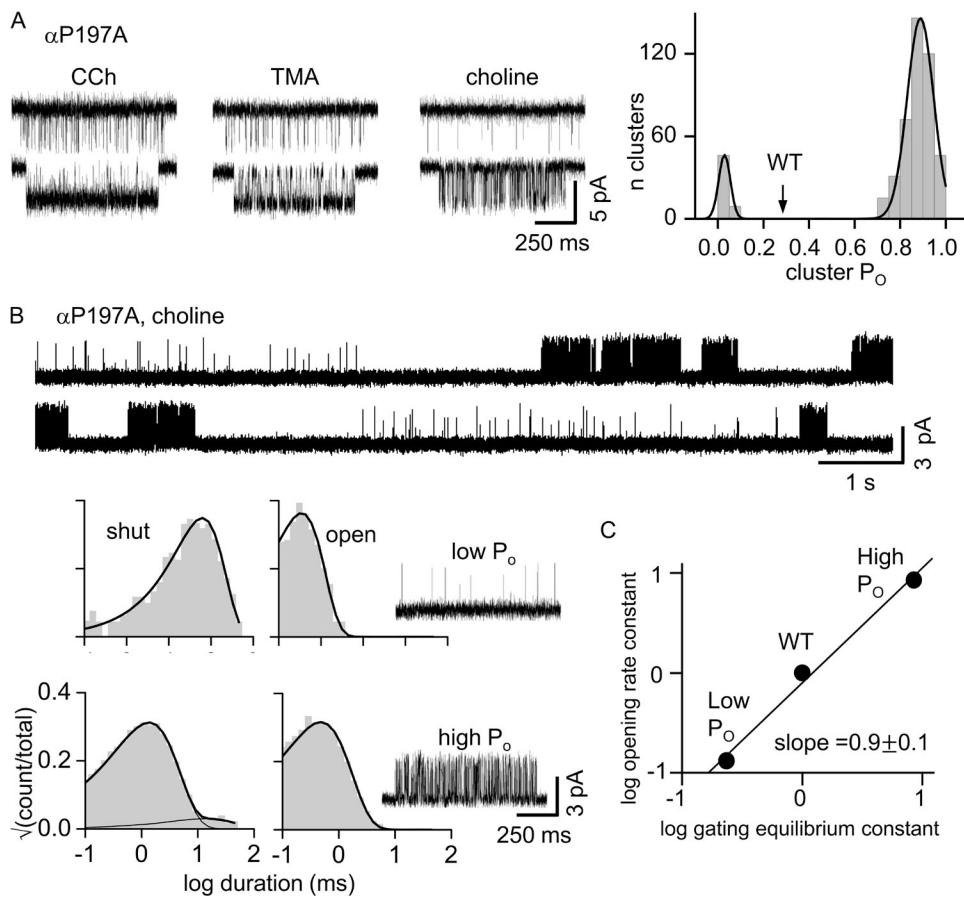


Figure 4. Partial agonists generate fewer modes than does ACh. (A; left) Example clusters for α P197A adult AChRs ([agonist] = 1 mM; -100 mV; open is down). (Right) Cluster P_O histogram for TMA with peaks at 0.04 ± 0.01 and 0.87 ± 0.10 . Arrow, P_O for TMA in WT AChRs (0.30 ± 0.06). The full agonist ACh has four P_O populations (Fig. 2 B, bottom). (B) α P197A adult AChRs activated by a saturating [Cho] (100 mM; 70 mV; open is up). (Top) Two modes are apparent. (Bottom left) Interval duration histograms and example clusters of each mode. (C) Phi (slope) analysis of α P197A choline modes. The fold-change in the di-liganded gating equilibrium constant is caused mainly by a similar fold-change in the channel-opening rate constant.

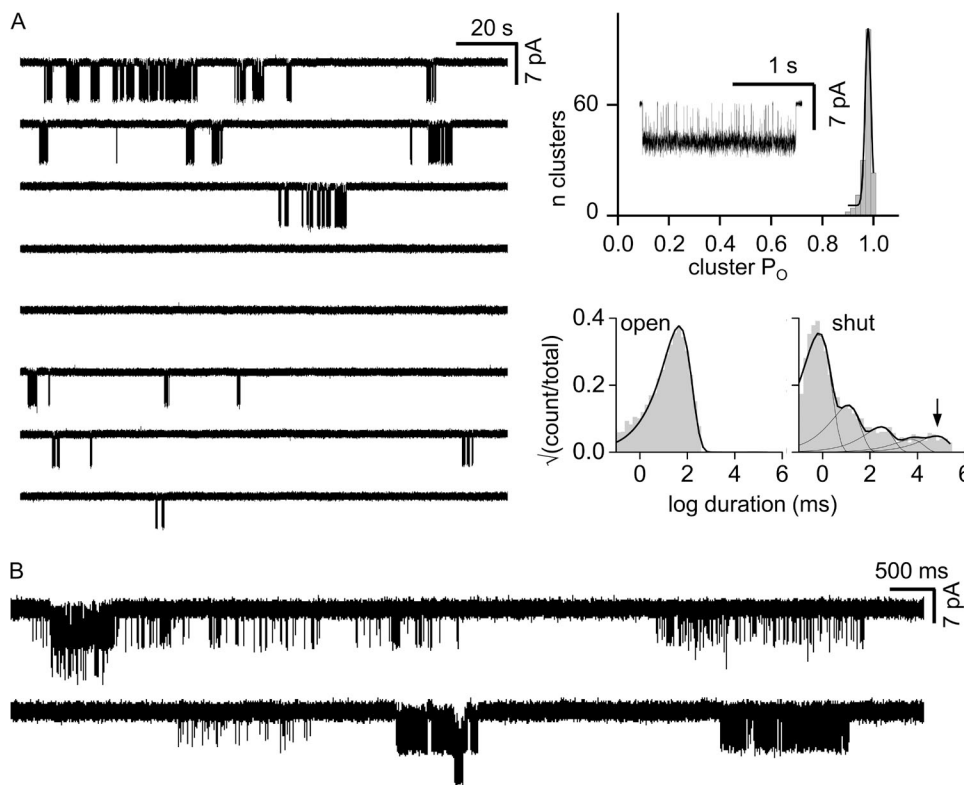


Figure 5. Modes are stable. (A; left) Low time-resolution view of α P197A (+ α Y93A) clusters from a patch having a single AChR. (Right) Corresponding histograms (adult AChR, 30 μ M ACh; -100 mV; open is down). For ~ 30 min, P_O was homogeneous. (Right, bottom) The slowest shut component (arrow; 162 ± 70 s), which represents recovery from deep desensitization, is similar to the WT value (270 s; Elenes and Auerbach, 2002), indicating that the patch probably had only one AChR. (B) A multichannel patch of the same construct shows P_O modes.

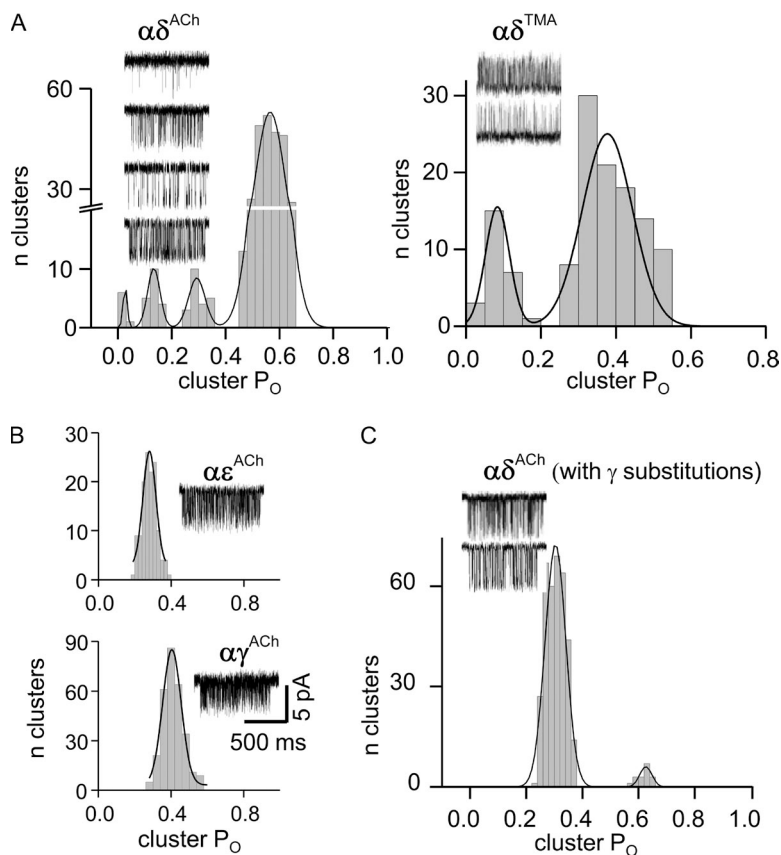


Figure 6. Modes are generated only at the $\alpha\delta$ agonist site. (A) With only a functional $\alpha\delta$ site there, are four P_{O}^{ACh} and two P_{O}^{TMA} populations, as in the WT. (B) Modes are absent in AChRs with only a functional $\alpha\epsilon$ or $\alpha\gamma$ site. (C) Substituting side chains from the γ subunit into the δ subunit (three in loop E and one in the $\beta 5$ – $\beta 5'$ linker; see Fig. 1) reduces modal activity. Open is down for ACh (-100 mV; 100 μ M for $\alpha\delta$ and $\alpha\epsilon$, and 30 μ M for $\alpha\gamma$) and up for TMA (70 mV; 5 mM).

This result indicates that the different P_{O}^{ACh} values apparent with agonist and the loop C proline mutations are generated by variations in K_d^{ACh} .

In the next set of experiments, we changed the agonist, using the $\alpha P197A$ mutation. With 1 mM of the partial agonists carbamylcholine, TMA, or choline, only two P_{O} populations were apparent, both different than the WT (Fig. 4 A).

We also measured the opening and closing rate constants for each of the $\alpha P197A$ modes using a saturating

[agonist] (Fig. 4 B). The difference in the di-liganded gating equilibrium constant between modes arose almost exclusively from a change in the opening rate constant (Fig. 4 C). This is characteristic of many α -subunit residues at the agonist sites (Purohit et al., 2013), and suggests that the structural perturbation responsible for the affinity variation is occurring locally, probably at loop C.

Regardless of the agonist, P_{O} was uniform within each cluster. We did not observe mode switching within $\sim 1,000$

TABLE 1
Affinity of modes at the $\alpha\delta$ site

Agonist	Mode	E_1^{obs}	E_1^{corr}	K_d	ΔG
				μM	<i>kcal/mol</i>
TMA	H	0.7	2.6×10^{-3}	25.8	-6.2
	L	0.004	1.5×10^{-5}	4,470	-3.2
ACh	HHH	3.7	0.09	0.74	-8.3
	HH	0.9	0.02	3.4	-7.4
	H	0.2	5×10^{-3}	13.4	-6.6
	L	0.01	2.5×10^{-4}	268	-4.8
ACh ^a	–	0.1	6.3×10^{-3}	10.6	-6.7

All AChRs had $\alpha P197A$ and the $\alpha\epsilon$ knockout mutation $\epsilon P121R$ (70 mV; $[TMA] = 5$ mM and $[ACh] = 10$ mM). Mode, H for high P_{O} and L for low P_{O} . E_1^{obs} , observed gating equilibrium constant with one agonist at the $\alpha\delta$ site; E_1^{corr} , gating equilibrium constant after correction for the background mutations; $K_d = (E_0^{WT}/E_1^{corr})$, where $E_0^{WT} = 6.7 \times 10^{-8}$ at 70 mV (Nayak et al., 2012); ΔG , $\alpha\delta$ -binding free energy ($+0.59 \ln K_d$). The adult WT, $\alpha\delta$ K_d values are: TMA (580 μ M; -4.4 kcal/mol) and ACh (175 μ M; -5.1 kcal/mol). Additional background mutations (total fold increase in E_0): TMA, $\epsilon L269F + \epsilon S450A$ (271); ACh, $\beta V266A$ (40), ACh^a, $\epsilon L269F$ (16).

^a $\delta W57A$ added to the background (WT value is $K_d^{ACh} = 80$ μ M; -5.6 kcal/mol (Nayak et al., 2014)).

α P197A clusters, which suggests that the time constant for mode switching is on the order of at least several minutes. By chance, we happened to record currents from a patch that had only a single AChR (Fig. 5 A). Although this construct showed heterogeneity in P_O^{ACh} in multi-channel patches (Fig. 5 B), in the one-channel patch, the clusters were homogeneous. In this experiment, the time scale for mode switching was more than ~ 30 min. In a one-channel patch, the long, closed intervals between clusters reflect desensitized periods of just that AChR (Elenes and Auerbach, 2002). The consistency of cluster P_O in this patch suggests that the affinity changes caused by α P197A are not associated with recovery from desensitization.

In all of the experiments described above, both AChR agonist sites were active and contributed to the cluster P_O . We next examined the properties of each agonist site separately ($\alpha\gamma$, $\alpha\delta$, or $\alpha\epsilon$). We added a binding site knockout mutation, in addition to a background mutation(s) that increased the allosteric constant, to allow the production of clusters and the measurement of P_O . Fig. 6 shows that with the α P197A mutation (in both α subunits) and ACh, the $\alpha\epsilon$ - and $\alpha\gamma$ -generated currents were homogeneous, but those arising from $\alpha\delta$ were modal. As in adult, two-site AChRs, the $\alpha\delta$ -only receptors produced four P_O^{ACh} populations and two P_O^{TMA} populations. This result suggests that all of the heterogeneity is caused by affinity variations at the $\alpha\delta$ site.

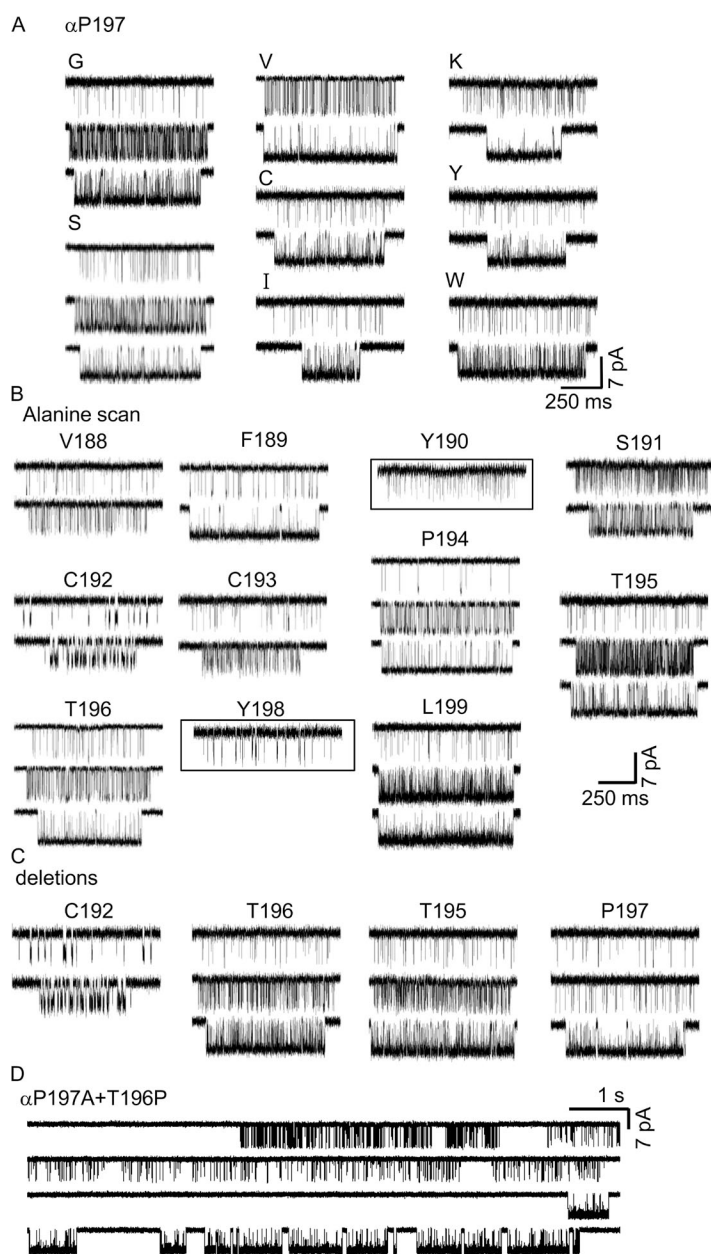


Figure 7. Example currents for α -subunit loop C perturbations. (A) Modes with different substitutions at α P197. For each mutation, examples of the various modes are shown directly below the mutant designation. Only two modes are apparent with larger side chains (see Fig. 2 for Ala mutation). (B) Alanine scan of loop C. Modes are apparent with an alanine substitution at every loop C position except α Y190 and α Y198 (boxed). (C) Deletions. Modes are present with deletions of some loop C residues. (D) Modes are present with α T196P added to the α P197A background. All experiments: adult AChRs, 30 μ M ACh; -100 mV; open is down.

To estimate the differences in affinity between modes at the $\alpha\delta$ site, we used a saturating concentration of agonist (Eq. 1 and Table 1). For TMA, the α P197A mutation resulted in AChRs having either an ~ 22 -fold higher affinity or an ~ 8 -fold lower affinity than the WT $\alpha\delta$ site. For ACh, three modes were higher affinity (by 2,326-, 51-, and 13-fold) and one was lower affinity (1.5-fold) than the WT. With both of these agonists, none of the α P197A-induced K_d values was the same as in the WT.

The results presented so far indicate that in endplate AChRs, α -loop C proline-to-alanine mutations (a) generate stable variations in resting affinity, (b) that are different from the WT, (c) for several different agonists, (d) only at the $\alpha\delta$ site, (e) by virtue of a local perturbation, and (f) by a mechanism that is independent of desensitization.

Mutations

To test whether or not modes are something specific to the proline-to-alanine loop C substitutions, we substituted different side chains at α P197. With ACh and in two-site adult AChRs, four modes were apparent with A, three with G and S, but only two with V, C, I, K, Y, and W (Fig. 7 A). This pattern suggests that larger side chain substitutions produce less heterogeneity.

We also substituted an alanine at each of the other loop C positions (Fig. 7 B). P_O^{ACh} heterogeneity was

present in all cases, with two exceptions. Mutation of either of the two loop C tyrosines that are part of the aromatic core (α Y190A and α Y198A) generated clusters that were homogeneous. Variation in affinity is not specific to mutations of the prolines.

We examined the properties of adult-type muscle AChRs having a deletion of one loop C amino acid (both α subunits). The deletion of α C192, α T195, α T196, or α P197 all resulted in modal P_O values (Fig. 7 C). We also replaced α T196 with a proline, on the α P197A background. This construct, too, produced multiple P_O^{ACh} values (Fig. 7 D).

In the next series of experiments, we examined the effects of mutating a core aromatic residue on α P197A-induced modes. Without this loop C mutation, an alanine substitution at α Y198 or α W149 decreases affinity to a similar extent (~ 30 -fold; ~ 2.0 kcal/mol) at all three agonist sites ($\alpha\epsilon$, $\alpha\delta$, and $\alpha\gamma$). In contrast, the effect of the complementary-side mutation W55A (it is position 57 in δ) is variable and reduces affinity by $\sim 2,000$ -fold (4.3 kcal/mol) at $\alpha\gamma$ and ~ 15 -fold (1.5 kcal/mol) at $\alpha\epsilon$, but at $\alpha\delta$ it increases affinity by twofold (-0.5 kcal/mol; Nayak et al., 2014).

To explore the role of this “variable” amino acid with regard to modes, we added δ W57A to α P197A and used ACh to activate AChRs having only a functional $\alpha\delta$ site (Fig. 8). The cluster P_O values were homogeneous, and

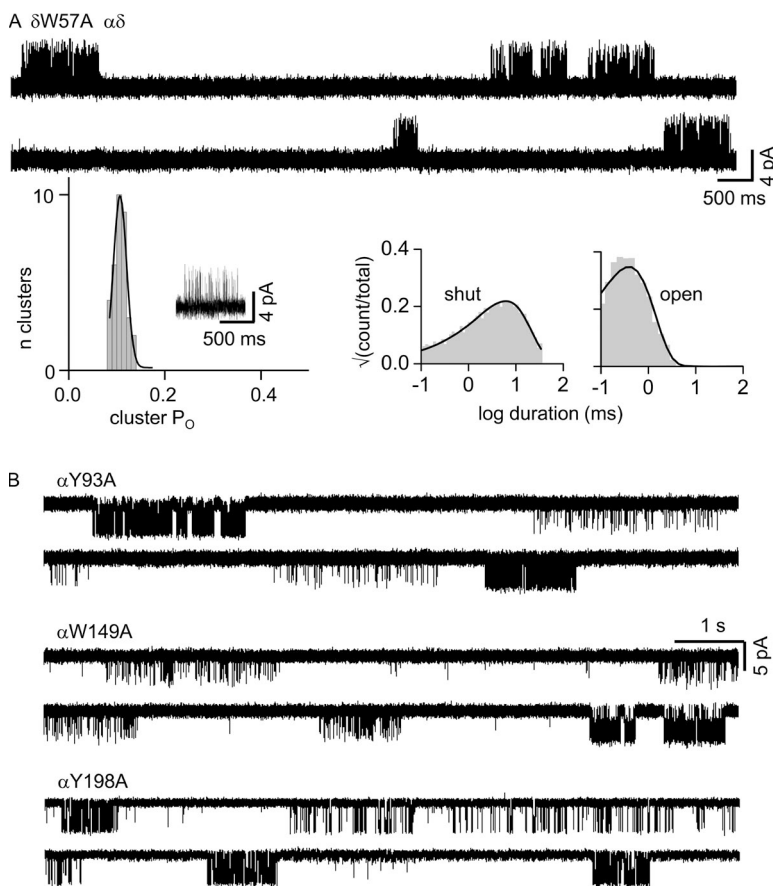


Figure 8. Alanine scan of the aromatic core. (A) δ W57A. (Top) Example currents from a single-site, $\alpha\delta$ -only AChR (3 mM ACh; 70 mV; open is up). (Bottom) Cluster P_O and interval duration histograms. Only one P_O population is apparent (K_d^{ACh} given in Table 1). (B) Example currents from other alanine mutants. Multiple modes are apparent (two-site, adult AChRs; 30 μ M ACh; -100 mV; open is down). α P197A was present for all.

K_d^{ACh} was lower than with a WT loop C (Table 1). Apparently, the $\delta W57$ mutation eliminates the alternative loop C conformations responsible for modes. $\alpha P197A$ modes were still apparent with an alanine substitution at $\alpha Y198$ (loop C), $\alpha W149$ (loop B), or $\alpha Y93$ (loop A).

We also counted modes from the $\alpha P197A$ mutation in AChRs activated by ACh and having only a functional $\alpha\delta$ site, but this time with an additional F mutation at one of the core aromatics (Fig. 9). An F mutation conserves the aromatic character of the side chain but removes H bonds made by the side chains. $\alpha P197A$ modal activity was eliminated or greatly reduced by $\alpha Y190F$, $\alpha Y198F$, and $\delta W57F$, but remained unaltered by $\alpha Y93F$.

In the final set of experiments, we analyzed the effects of mutations to δ subunit amino acids on the complementary β sheet (Fig. 1). Recently, it was discovered that low-affinity $\alpha\delta$ and high-affinity $\alpha\gamma$ binding energies can be exchanged by swapping four complementary side chains, three in loop E ($\delta Y113$, $\delta D114$, and $\delta S115$) and one in the $\beta 5$ – $\beta 5'$ linker, near $\alpha W149$ ($\delta Y106$; unpublished data). Because $\alpha\gamma$ alone does not exhibit modes, we investigated the effects of exchanging these four side chains on $\alpha\delta$ modal activity. We replaced these four side chains in δ with the corresponding ones from γ , and observed that the $\alpha P197A$ -induced modes with ACh were greatly reduced (Fig. 6 C).

The mutational analyses suggest that (a) almost all perturbations of loop C unsettle $\alpha\delta$ affinity, (b) $\delta W57$ is

a source of the affinity variations, (c) H-bonding patterns at the aromatic core influence the variations, and (d) loop E and the $\beta 5$ – $\beta 5'$ linker in the δ subunit contribute to modal activity.

DISCUSSION

In muscle nicotinic AChRs, almost all α -subunit loop C perturbations cause modal gating activity, with the P_O differences generated by variations in K_d at the $\alpha\delta$ agonist site. To explore a potential mechanism, we begin with some assumptions and inferences based on experimental observations.

In AChRs, K_d is determined by diffusion of the agonist to a binding site and a local, conformation change at the agonist site (Jadey and Auerbach, 2012). We assume that modes reflect differences in the equilibrium constant of this conformational change (“catch”) rather than diffusion. K_d is determined mainly by the interaction of aromatic side chains at the core with the ligand’s quaternary amino group (Kearney et al., 1996; Zhong et al., 1998; Beene et al., 2002). We assume that different affinities reflect relatively different positions of the quaternary amino within the aromatic core (Bruhova et al., 2013). A difference in binding energy can be associated with a difference in conformation (structure, dynamics, or both), but the converse is not necessarily true because different conformations can generate identical affinities. Nonetheless, we assume a one-to-one correspondence

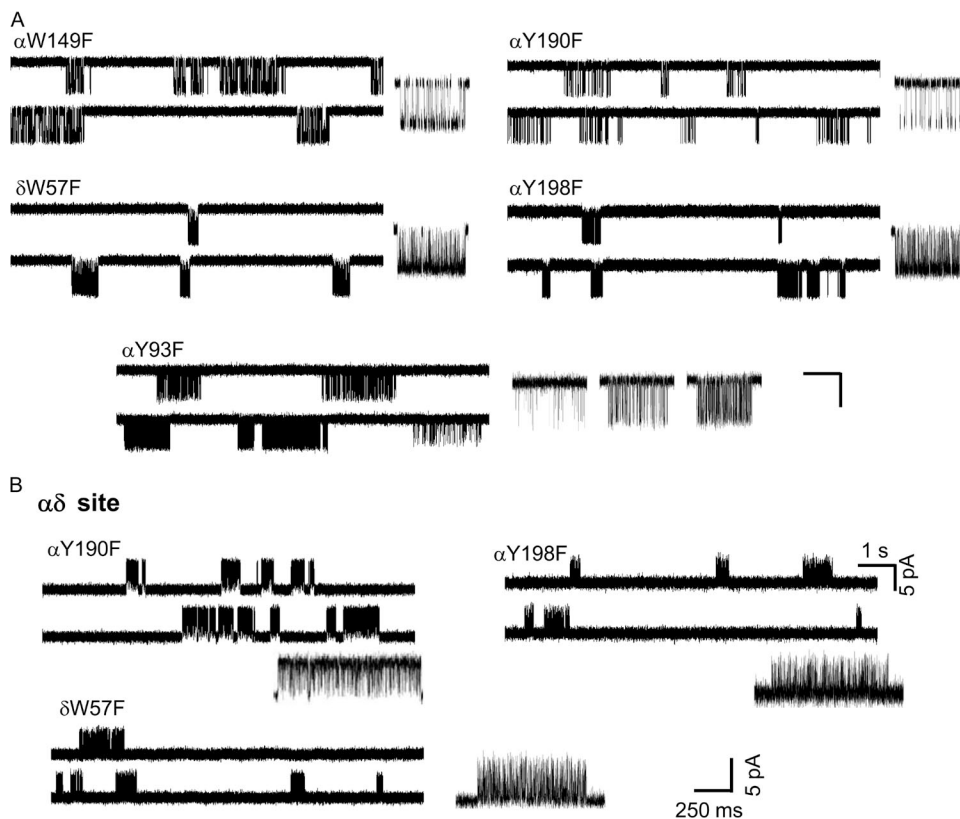


Figure 9. Phenylalanine scan of the aromatic core. (A) All F substitutions eliminate $\alpha P197A$ modes except for $\alpha Y93F$ (two-site, adult AChRs; 30 μM ACh; -100 mV; open is down). Calibration, 1 s/7 pA (low resolution traces) and 250 ms, 5 pA (high resolution clusters). (B) F substitutions at one-site, $\alpha\delta$ -only AChRs (3 mM ACh; 70 mV; open is up). Clusters from $\alpha Y190F$, $\alpha Y198F$, and $\delta W57F$ are homogeneous.

between conformation and K_d , because of the high sensitivity of the measurements and because the P_O distributions are approximately Gaussian. Based on these three assumptions, we conclude that in WT AChRs, there is (approximately) one catch conformation, and that perturbing loop C of the α subunit allows for more than one.

α P197A modes are stable on a time scale of minutes (Fig. 5), which implies that the free energy barriers separating alternative catch conformations are large. We infer that each mode represents a different, stable K_d conformation. These conformations may reflect different protein folds or different posttranslational modifications. Modes are generated by almost all α -loop C perturbations (Fig. 7). This result implies that the conformational uniformity of the WT binding pocket is readily disrupted by altering loop C. We cannot be sure that the WT α -loop C sequence is the only “golden” one, but it appears that residues here have been selected to enforce a single affinity, perhaps to increase the reliability of the endplate current. Loop C is involved in agonist binding and has high-phi for gating (like modes; Fig. 4 C), and so far it is the main structural element associated with mode generation. We infer that differences in α -subunit loop C structure/dynamics motivate the alternative K_d conformations. Modes arise exclusively from the $\alpha\delta$ site and are reduced by swapping loop E side chains, δ -to- γ (Fig. 6). We infer that alternative conformations of the complementary subunit (for short, the ‘ β -sheet’) are also involved in mode generation.

There are four modes apparent with α P197A and ACh (Figs. 2 B and 6 A). A simple interpretation, based on the above assumptions and inferences, is that two structural elements—the α -loop C and the δ -subunit β sheet—each can adopt two alternative K_d conformations. With the α P197A mutation, none of the K_d values are the same as in the WT (Table 1). We hypothesize that none of the four possible catch conformations are the same as in the WT. We call this a 2×2 mechanism.

Undoubtedly, the situation is more complex. First, loop C of the α subunit and the β sheet of the non- α subunit do not operate independently. Interactions between the α and δ subunits can occur through side chains, the agonist itself, a structural water in the pocket (Amiri et al., 2007; Olsen et al., 2014), intersubunit H bonds, as well as through backbone breathing motions (Taly et al., 2005). Second, each of the two structural elements in the 2×2 model is complex. Loop C interacts with other loops in the α -subunit site of the binding pocket, and the non- α -subunit surface is a super-secondary structure having several components (β sheet, $\beta 5'$ - $\beta 6$ hairpin turn, $\beta 5$ - $\beta 5'$ linker, and a structural water; Fig. 1). Given this complexity, it is difficult to dissect unambiguously the possible route(s) for mode generation. Nonetheless, we will use the simple 2×2 model as the starting point for interpreting the experimental results.

(a) α P197A induces four modes with ACh but only two for the partial agonists TMA, carbamylcholine, and choline. The partial agonists probably do not H bond across the subunit interface or with the structural water. We speculate that these ligands do not have this α - δ link, and therefore that α P197A allows the two loop C conformations, but not those of the β sheet. The agonist and structural water appear to participate in K_d variation.

(b) With ACh, only two modes are apparent with V, C, I, K, Y, and W mutations of α P197 (Fig. 7). We speculate that having a large side chain here favors one of the alternative loop C conformations that nonetheless allows for two conformations of the β sheet. Steric bumping with other loops at the binding pocket (Grutter et al., 2003) appears to play a role in K_d variation.

(c) An alanine mutation of all loop C residues generates modes except for the two loop C tyrosines that “clamp” the agonist in the pocket. This result suggests that all three elements of this clamp are required for loop C to adopt alternative conformations. We speculate that with only one tyrosine, α -loop C adopts a single, preferred conformation that does not allow β -sheet alternatives. The two loop C tyrosines are involved in mode generation.

(d) α P197 modes are eliminated by an A substitution at core residue δ W57 but not at α W149, α Y198, or α Y93. This complicates the model because it makes β -sheet residue δ W57 an instigator of, rather than a responder to, α -loop C alternatives. If δ W57 is simply one element of the β -sheet alternatives, the 2×2 model predicts two modes (the loop C alternatives), whereas only one was apparent. Hence, δ W57 either interacts with loop C to alter its conformational flexibility (which is surprising, because this side chain has almost no effect on affinity in the WT), or can take on alternative positions that result in the same affinity for different loop C configurations (violating assumption c, above). δ W57 appears to be an important and variable source for the modal differences in agonist-binding energy.

(e) α P197A modes are reduced by δ -subunit mutations in loop E and the $\beta 5$ - $\beta 5'$ linker. The loop E mutations change H-bond patterns and backbone dynamics of the β sheet to influence the participation of δ W57 (unpublished data). The flexibility of the $\beta 5'$ - $\beta 6$ hairpin may also influence K_d modes.

(f) α P197A modes are greatly reduced by an F substitution at α Y190, α Y198, α W149, and δ W57 but not α Y93. This suggests that the complete network of H bonds formed by the two loop C tyrosine-OH groups and the two indole nitrogen atoms is required for mode generation by α P197A. We cannot speculate further, except to propose that variation in H bonding, too, is involved in K_d variability.

It has been 30 years since P_O modes were first reported for AChRs. Here, we have shown that these arise from stable differences in affinity, at the $\alpha\delta$ agonist site, as

influenced by loop C and the complementary β sheet. The ligand, a structural water, $\delta W57$, loop E, and H bonds at the core of the $\alpha\delta$ site all appear to participate. The agonist-binding apparatus is intricate and entangled. More and different kinds of experiments may be required to fully reveal the molecular mechanism(s) that undergirds the modal affinities of endplate AChRs.

We thank Marlene Shero, Mary Merritt, and Mary Teeling for technical assistance.

This work was funded by the National Institutes of Health (grant NS064969).

The authors declare no competing financial interests.

Kenton J. Swartz served as editor.

Submitted: 26 August 2015

Accepted: 5 October 2015

REFERENCES

- Amiri, S., M.S. Sansom, and P.C. Biggin. 2007. Molecular dynamics studies of AChBP with nicotine and carbamylcholine: the role of water in the binding pocket. *Protein Eng. Des. Sel.* 20:353–359. <http://dx.doi.org/10.1093/protein/gzm029>
- Auerbach, A. 2012. Thinking in cycles: MWC is a good model for acetylcholine receptor-channels. *J. Physiol.* 590:93–98. <http://dx.doi.org/10.1113/jphysiol.2011.214684>
- Auerbach, A., and C.J. Lingle. 1986. Heterogeneous kinetic properties of acetylcholine receptor channels in *Xenopus* myocytes. *J. Physiol.* 378:119–140. <http://dx.doi.org/10.1113/jphysiol.1986.sp016211>
- Beene, D.L., G.S. Brandt, W. Zhong, N.M. Zacharias, H.A. Lester, and D.A. Dougherty. 2002. Cation- π interactions in ligand recognition by serotonergic (5-HT_{3A}) and nicotinic acetylcholine receptors: the anomalous binding properties of nicotine. *Biochemistry.* 41:10262–10269. <http://dx.doi.org/10.1021/bi020266d>
- Blatz, A.L., and K.L. Magleby. 1986. Quantitative description of three modes of activity of fast chloride channels from rat skeletal muscle. *J. Physiol.* 378:141–174. <http://dx.doi.org/10.1113/jphysiol.1986.sp016212>
- Bruhova, I., T. Gregg, and A. Auerbach. 2013. Energy for wild-type acetylcholine receptor channel gating from different choline derivatives. *Biophys. J.* 104:565–574. <http://dx.doi.org/10.1016/j.bpj.2012.11.3833>
- Chakrapani, S., J.F. Cordero-Morales, V. Jogini, A.C. Pan, D.M. Cortes, B. Roux, and E. Perozo. 2011. On the structural basis of modal gating behavior in K⁺ channels. *Nat. Struct. Mol. Biol.* 18:67–74. <http://dx.doi.org/10.1038/nsmb.1968>
- Elenes, S., and A. Auerbach. 2002. Desensitization of diliganded mouse muscle nicotinic acetylcholine receptor channels. *J. Physiol.* 541:367–383. <http://dx.doi.org/10.1113/jphysiol.2001.016022>
- Grutter, T., L. Prado de Carvalho, N. Le Novère, P.J. Corringer, S. Edelstein, and J.P. Changeux. 2003. An H-bond between two residues from different loops of the acetylcholine binding site contributes to the activation mechanism of nicotinic receptors. *EMBO J.* 22:1990–2003. <http://dx.doi.org/10.1093/emboj/cdg197>
- Gupta, S., P. Purohit, and A. Auerbach. 2013. Function of interfacial prolines at the transmitter-binding sites of the neuromuscular acetylcholine receptor. *J. Biol. Chem.* 288:12667–12679. <http://dx.doi.org/10.1074/jbc.M112.443911>
- Hurdiss, E.J., T. Greiner, R. Yu, P.C. Biggin, and L.G. Sivilotti. 2015. The kinetic properties of the human glycine receptor in response to different agonists. *Biophys. J.* 108:432a. <http://dx.doi.org/10.1016/j.bpj.2014.11.2360>
- Ionescu, L., C. White, K.H. Cheung, J. Shuai, I. Parker, J.E. Pearson, J.K. Foskett, and D.O.D. Mak. 2007. Mode switching is the major mechanism of ligand regulation of InsP₃ receptor calcium release channels. *J. Gen. Physiol.* 130:631–645. <http://dx.doi.org/10.1085/jgp.200709859>
- Jackson, M.B. 1986. Kinetics of unliganded acetylcholine receptor channel gating. *Biophys. J.* 49:663–672. [http://dx.doi.org/10.1016/S0006-3495\(86\)83693-1](http://dx.doi.org/10.1016/S0006-3495(86)83693-1)
- Jadey, S., and A. Auerbach. 2012. An integrated catch-and-hold mechanism activates nicotinic acetylcholine receptors. *J. Gen. Physiol.* 140:17–28. <http://dx.doi.org/10.1085/jgp.201210801>
- Jadey, S.V., P. Purohit, I. Bruhova, T.M. Gregg, and A. Auerbach. 2011. Design and control of acetylcholine receptor conformational change. *Proc. Natl. Acad. Sci. USA.* 108:4328–4333. <http://dx.doi.org/10.1073/pnas.1016617108>
- Kearney, P.C., M.W. Nowak, W. Zhong, S.K. Silverman, H.A. Lester, and D.A. Dougherty. 1996. Dose-response relations for unnatural amino acids at the agonist binding site of the nicotinic acetylcholine receptor: tests with novel side chains and with several agonists. *Mol. Pharmacol.* 50:1401–1412.
- Lema, G.M., and A. Auerbach. 2006. Modes and models of GABA(A) receptor gating. *J. Physiol.* 572:183–200. <http://dx.doi.org/10.1113/jphysiol.2005.099093>
- Magleby, K.L. 2004. Modal gating of NMDA receptors. *Trends Neurosci.* 27:231–233. <http://dx.doi.org/10.1016/j.tins.2004.03.001>
- McManus, O.B., and K.L. Magleby. 1988. Kinetic states and modes of single large-conductance calcium-activated potassium channels in cultured rat skeletal muscle. *J. Physiol.* 402:79–120. <http://dx.doi.org/10.1113/jphysiol.1988.sp017195>
- Naranjo, D., and P. Brehm. 1993. Modal shifts in acetylcholine receptor channel gating confer subunit-dependent desensitization. *Science.* 260:1811–1814. <http://dx.doi.org/10.1126/science.8511590>
- Nayak, T.K., P.G. Purohit, and A. Auerbach. 2012. The intrinsic energy of the gating isomerization of a neuromuscular acetylcholine receptor channel. *J. Gen. Physiol.* 139:349–358. <http://dx.doi.org/10.1085/jgp.201110752>
- Nayak, T.K., I. Bruhova, S. Chakraborty, S. Gupta, W. Zheng, and A. Auerbach. 2014. Functional differences between neurotransmitter binding sites of muscle acetylcholine receptors. *Proc. Natl. Acad. Sci. USA.* 111:17660–17665. <http://dx.doi.org/10.1073/pnas.1414378111>
- Nicolai, C., and F. Sachs. 2013. Solving ion channel kinetics with the QuB software. *Biophys. Rev. Lett.* 08:191–211. <http://dx.doi.org/10.1142/S1793048013300053>
- Nilius, B. 1987. Modal gating behaviour of single sodium channels from the guinea-pig heart. *Biomed. Biochim. Acta.* 46:S662–S667.
- Olsen, J.A., T. Balle, M. Gajhede, P.K. Ahring, and J.S. Kastrop. 2014. Molecular recognition of the neurotransmitter acetylcholine by an acetylcholine binding protein reveals determinants of binding to nicotinic acetylcholine receptors. *PLoS One.* 9:e91232. <http://dx.doi.org/10.1371/journal.pone.0091232>
- Poon, K., L.M. Nowak, and R.E. Oswald. 2010. Characterizing single-channel behavior of GluA3 receptors. *Biophys. J.* 99:1437–1446. <http://dx.doi.org/10.1016/j.bpj.2010.06.058>
- Popescu, G., and A. Auerbach. 2003. Modal gating of NMDA receptors and the shape of their synaptic response. *Nat. Neurosci.* 6:476–483.
- Prieto, M.L., and L.P. Wollmuth. 2010. Gating modes in AMPA receptors. *J. Neurosci.* 30:4449–4459. <http://dx.doi.org/10.1523/JNEUROSCI.5613-09.2010>
- Purohit, P., and A. Auerbach. 2009. Unliganded gating of acetylcholine receptor channels. *Proc. Natl. Acad. Sci. USA.* 106:115–120. <http://dx.doi.org/10.1073/pnas.0809272106>
- Purohit, P., and A. Auerbach. 2010. Energetics of gating at the apo-acetylcholine receptor transmitter binding site. *J. Gen. Physiol.* 135:321–331. <http://dx.doi.org/10.1085/jgp.200910384>

- Purohit, P., and A. Auerbach. 2013. Loop C and the mechanism of acetylcholine receptor-channel gating. *J. Gen. Physiol.* 141:467–478. <http://dx.doi.org/10.1085/jgp.201210946>
- Purohit, P., I. Bruhova, and A. Auerbach. 2012. Sources of energy for gating by neurotransmitters in acetylcholine receptor channels. *Proc. Natl. Acad. Sci. USA.* 109:9384–9389. <http://dx.doi.org/10.1073/pnas.1203633109>
- Purohit, P., S. Gupta, S. Jadey, and A. Auerbach. 2013. Functional anatomy of an allosteric protein. *Nat. Commun.* 4:2984. <http://dx.doi.org/10.1038/ncomms3984>
- Purohit, P., I. Bruhova, S. Gupta, and A. Auerbach. 2014. Catch-and-hold activation of muscle acetylcholine receptors having transmitter binding site mutations. *Biophys. J.* 107:88–99. <http://dx.doi.org/10.1016/j.bpj.2014.04.057>
- Sakmann, B., J. Patlak, and E. Neher. 1980. Single acetylcholine-activated channels show burst-kinetics in presence of desensitizing concentrations of agonist. *Nature.* 286:71–73. <http://dx.doi.org/10.1038/286071a0>
- Smith, M.A., and M.L. Ashford. 1998. Mode switching characterizes the activity of large conductance potassium channels recorded from rat cortical fused nerve terminals. *J. Physiol.* 513:733–747. <http://dx.doi.org/10.1111/j.1469-7793.1998.733ba.x>
- Taly, A., M. Delarue, T. Grutter, M. Nilges, N. Le Novère, P.-J. Corringer, and J.-P. Changeux. 2005. Normal mode analysis suggests a quaternary twist model for the nicotinic receptor gating mechanism. *Biophys. J.* 88:3954–3965. <http://dx.doi.org/10.1529/biophysj.104.050229>
- Zhang, W., J.R. Howe, and G.K. Popescu. 2008. Distinct gating modes determine the biphasic relaxation of NMDA receptor currents. *Nat. Neurosci.* 11:1373–1375. <http://dx.doi.org/10.1038/nn.2214>
- Zhong, W., J.P. Gallivan, Y. Zhang, L. Li, H.A. Lester, and D.A. Dougherty. 1998. From ab initio quantum mechanics to molecular neurobiology: a cation- π binding site in the nicotinic receptor. *Proc. Natl. Acad. Sci. USA.* 95:12088–12093. <http://dx.doi.org/10.1073/pnas.95.21.12088>